



Stabilized linear semi-implicit schemes for the nonlocal Cahn–Hilliard equation

Qiang Du^a, Lili Ju^b, Xiao Li^{c,*}, Zhonghua Qiao^d

^a Department of Applied Physics and Applied Mathematics, Columbia University, New York, NY 10027, USA

^b Department of Mathematics, University of South Carolina, Columbia, SC 29208, USA

^c Applied and Computational Mathematics Division, Beijing Computational Science Research Center, Beijing 100193, China

^d Department of Applied Mathematics, The Hong Kong Polytechnic University, Hung Hom, Kowloon, Hong Kong



ARTICLE INFO

Article history:

Received 20 October 2017

Received in revised form 5 February 2018

Accepted 9 February 2018

Available online 14 February 2018

Keywords:

Nonlocal Cahn–Hilliard equation

Nonlocal diffusion operator

Stabilized linear scheme

Fast Fourier transform

Energy stability

Gaussian kernel

ABSTRACT

Comparing with the well-known classic Cahn–Hilliard equation, the nonlocal Cahn–Hilliard equation is equipped with a nonlocal diffusion operator and can describe more practical phenomena for modeling phase transitions of microstructures in materials. On the other hand, it evidently brings more computational costs in numerical simulations, thus efficient and accurate time integration schemes are highly desired. In this paper, we propose two energy-stable linear semi-implicit methods with first and second order temporal accuracies respectively for solving the nonlocal Cahn–Hilliard equation. The temporal discretization is done by using the stabilization technique with the nonlocal diffusion term treated implicitly, while the spatial discretization is carried out by the Fourier collocation method with FFT-based fast implementations. The energy stabilities are rigorously established for both methods in the fully discrete sense. Numerical experiments are conducted for a typical case involving Gaussian kernels. We test the temporal convergence rates of the proposed schemes and make a comparison of the nonlocal phase transition process with the corresponding local one. In addition, long-time simulations of the coarsening dynamics are also performed to predict the power law of the energy decay.

© 2018 Elsevier Inc. All rights reserved.

1. Introduction

Mesoscopic descriptions of phase transition are often modeled under the assumption that the evolution of the order parameter follows a gradient flow of the free energy with respect to certain metric. In the case of binary materials, a particular form of the free energy functional could be written as follows [6]

$$E(u) = \int_{\Omega} \left(F(u(\mathbf{x})) + \frac{\varepsilon^2}{4} \int_{\Omega} J(\mathbf{x} - \mathbf{y})(u(\mathbf{x}) - u(\mathbf{y}))^2 d\mathbf{y} \right) d\mathbf{x}, \quad (1)$$

where $\varepsilon > 0$ is an interface parameter, $\Omega \subset \mathbb{R}^d$ is a spatial domain ($d = 1, 2$, or 3), and $u(\mathbf{x})$ represents the scaled concentration or an order parameter of one component. The first term of the integrand in (1) represents the homogeneous free energy density and F is usually a double well function. The second term plays a role as the interaction energy density,

* Corresponding author.

E-mail addresses: qd2125@columbia.edu (Q. Du), ju@math.sc.edu (L. Ju), xiaoli@csra.ac.cn (X. Li), zhonghua.qiao@polyu.edu.hk (Z. Qiao).

representing the long-range interactions between atoms at different lattice sites, where J denotes an interaction kernel. In [33], the integral form of the nonlocal interactions has been attributed back to van der Waals [42]. The nonlocal Cahn–Hilliard (NCH) equation to be considered in this paper is resulted from the energetic variation of the energy functional (1) with F a double well quartic function in the H^{-1} Sobolev space. The specific form of the model equation as well as some assumptions on the kernel will be given in the next section.

It is well-known that the classic Cahn–Hilliard equation [10] is one of typical systems of the phase field models and has been successfully applied to describe the phase separations occurring in mixtures consisting of small molecules and some other interface problems involving mass-conserved order parameters. Recently, the NCH equation has attracted more and more attentions and used in many fields ranging from physics, materials science to finance and image processing. In materials science, the NCH equation and other related equations arise as mesoscopic models of interacting particle systems [2,26] and are taken to model phase transitions [20]. In the dynamic density functional theory [1,2], the interaction kernel J is the two-particle direct correlation function and u represents the mesoscopic particle density. In mathematical models of finance, the kernel arises from an expectation taken with respect to a particular measure used in option pricing [32]. In models for image segmentation with the NCH equation, the kernel is interpreted as the attracting force [21].

There have been many works on both mathematical and numerical aspects for the nonlocal models. On the mathematical analysis, the well-posedness of the NCH equations equipped with Neumann or Dirichlet boundary condition were investigated by Bates and Han [7,8] by assuming the integrability of the kernel. Guan et al. pointed out in [24] that the existence and uniqueness of the periodic solution to the NCH equation may be established using the similar techniques. Fife [20] surveyed some parabolic-like evolution equations including nonlocal and pattern-forming problems and made a brief comparison between the local and nonlocal equations. To develop a general framework of nonlocal models, Du et al. [14] analyzed a class of nonlocal diffusion problems with volume constrained boundary conditions, which are the nonlocal versions of classic diffusion problems with local boundary constraints, and a number of examples ranging from continuum mechanics to graph theory were showed to be special cases of the nonlocal models. On the numerical discretization, Bates et al. [5] developed an L^∞ stable and convergent numerical scheme for the nonlocal Allen–Cahn equation, the L^2 gradient flow with respect to (1), by treating the nonlinear and nonlocal terms explicitly. A similar approach was used on the nonlocal Allen–Cahn type problem coupled with a heat equation [3] and an L^∞ stable and convergent numerical scheme was obtained. For the nonlocal diffusion models with variable boundary conditions, finite element approximations were addressed in [39,45]. To illustrate the limit behavior of the computed solution of the nonlocal model to the exact solution of the corresponding local one, Tian and Du [40] proposed the concept on asymptotic compatibility, and the spectral-Galerkin approximations of the nonlocal Allen–Cahn equations were then proved to be asymptotically compatible.

Due to the energetic variational structure of the underlying model, the energy of the exact solutions to the NCH equations decreases in time. Thus, a significant issue in numerical simulations of the NCH equations is to develop algorithms inheriting this property at the discrete level. The algorithms of this type are usually called to be *energy stable*. Energy stability has been widely investigated for numerical schemes of a family of classic PDE-based phase field models, such as convex splitting schemes [34,36,43], stabilized schemes [38,44], exponential time differencing schemes [27,28], auxiliary variable methods [35] and so on. It is interesting to study if similar analysis can be applied to nonlocal phase field models due to the lack of the high-order diffusion term. As we will show later, the NCH equation could be obtained by replacing the Laplacian operator in the classic Cahn–Hilliard equation by a nonlocal diffusion operator resulted from the energetic variation of the nonlocal interaction term in the energy functional (1), thus it seems natural to consider the convex splitting schemes under the framework exploited by Eyre [19] for the local Cahn–Hilliard equation. The convex splitting schemes are unconditionally energy stable but often have to be solved iteratively at each time step due to implicit treatment of the nonlinearity. Thus, when the nonlocal term is put in the implicit part, one must compute it in each nonlinear iteration at each time step, which increases the computational cost. Based on this observation, Guan et al. [22–24] constructed a convex splitting scheme in an alternative way by treating the nonlinear term implicitly and putting the nonlocal term into the explicit part. Their scheme allows one to evaluate the nonlocal term explicitly only once at each time step, which is a good improvement over standard schemes, but the iterations are still inevitable.

A major motivation for us to study stabilized linear schemes for the NCH equations lies in the fact that, if we have linear schemes with the nonlocal term in the implicit level, then we are able to solve the fully discrete system efficiently in the frequency space via the spectral discretization and the fast Fourier transform (FFT) technique. In this paper, we will present and analyze two *linear* schemes for solving the NCH equation by using stabilized semi-implicit time discretization combined with the Fourier collocation method for spatial approximation. Such methods have been studied by many researchers in other contexts. For example, semi-implicit time-stepping was used by Chen and Shen [11] for phase field simulations. Stabilized method was also used by Xu and Tang [44] to develop energy stable schemes for the epitaxial growth model. A first order linear semi-implicit scheme was given by adding a stabilization term of the form $A\Delta_h(u_h^{n+1} - u_h^n)$, where the stabilizing parameter A depends nonlinearly on the numerical solutions. Tang et al. [25] also applied the same technique on the classic Cahn–Hilliard equation and again the L^∞ bound assumption on u_h^{n+1} was implicitly used to make A controllable. Similar approaches were utilized on the Allen–Cahn and Cahn–Hilliard equations [38] by assuming the Lipschitz continuity of the derivative of the potential. The linear convex splitting scheme presented in [12] for the epitaxial growth model was essentially a first order stabilized semi-implicit scheme with the stabilizer equal to one. In the recent works [29,30], the technical restrictions on A were removed and a more reasonable stability theory was established for phase field models like the Cahn–Hilliard equations. The work in this paper is motivated partly by the fact that the stabilized semi-implicit

schemes mentioned above are linear (thus more efficient than nonlinear schemes) and energy stable. To the best of our knowledge, this represents the first investigation on the application of the linear stabilization strategy to the nonlocal phase field models.

The rest of the paper is organized as follows. In Section 2, we briefly introduce the NCH equation and illustrate its connection to the classic Cahn–Hilliard equation. Spectral collocation and definitions of some discrete spatial operators are given in Section 3. In Section 4, the first and second order stabilized semi-implicit schemes are developed and analyzed; in particular, their energy stabilities are proved rigorously in the fully discrete form. Note that although the analysis in Sections 3 and 4 are done only for the 2D case, similar results can be obtained for the 1D and 3D cases without any extra essential difficulties. In Section 5, we first specialize the nonlocal model to the one involving a class of Gaussian kernels parameterized by a horizon number δ . Under different values of (ε, δ) , we numerically test temporal accuracies of the proposed schemes and compare the nonlocal phase transition processes with the corresponding local ones. In addition, long-time simulations of the coarsening dynamics are also performed to predict the power law of the energy decay rate. Finally, some concluding remarks are given in Section 6.

2. The nonlocal Cahn–Hilliard equation

We now give a brief review of the NCH equation associated with the energy functional (1) and its connection to the classic Cahn–Hilliard equation. Let us consider $\Omega = \prod_{i=1}^d (-X_i, X_i)$, a rectangular cell in \mathbb{R}^d . It is assumed throughout the paper that the kernel J always satisfies the following conditions:

- (a) $J(\mathbf{x}) \geq 0$ for any $\mathbf{x} \in \Omega$,
- (b) J is a radial function, i.e., $J(\mathbf{x}) = j(|\mathbf{x}|)$ for some single-variable function j ,
- (c) J is Ω -periodic,
- (d) $\frac{1}{2} \int_{\Omega} J(\mathbf{x}) |\mathbf{x}|^2 d\mathbf{x} = 1$.

Note that the condition (d) means that J has a finite second moment in Ω . Denote by $\|\cdot\|_{L^p}$ the spatial $L^p(\Omega)$ norm for $1 \leq p \leq \infty$ and by $L^p_{\text{per}}(\Omega)$ the space of all periodic functions in $L^p(\Omega)$. For simplicity, the usual L^2 norm and L^2 inner product are denoted by $\|\cdot\|$ and (\cdot, \cdot) , respectively.

2.1. Nonlocal operator and nonlocal Cahn–Hilliard equation

Let us define the nonlocal linear operator $\mathcal{L} : L^2_{\text{per}}(\Omega) \rightarrow L^2_{\text{per}}(\Omega)$ as

$$\mathcal{L} : v(\mathbf{x}) \mapsto \int_{\Omega} J(\mathbf{x} - \mathbf{y})(v(\mathbf{x}) - v(\mathbf{y})) d\mathbf{y}, \quad (2)$$

then we know that \mathcal{L} is self-adjoint and positive semi-definite under the above assumptions. Moreover, by acting \mathcal{L} on $\exp(i\tilde{\mathbf{k}} \cdot \mathbf{x})$ where $\tilde{\mathbf{k}} = (\tilde{k}_1, \dots, \tilde{k}_d)$ with $\tilde{k}_i = k_i \pi / X_i$ and $k_i \in \mathbb{Z}$, the basis functions on $L^2_{\text{per}}(\Omega)$, we can obtain the eigenvalues $\{\Lambda_{\mathbf{k}} : \mathbf{k} \in \mathbb{Z}^d\}$ of \mathcal{L} given by

$$\Lambda_{\mathbf{k}} = \int_{\Omega} J(\mathbf{x}) (1 - \exp(-i\tilde{\mathbf{k}} \cdot \mathbf{x})) d\mathbf{x} = \int_{\Omega} J(\mathbf{x}) (1 - \cos(\tilde{\mathbf{k}} \cdot \mathbf{x})) d\mathbf{x} \geq 0. \quad (3)$$

By some simple calculations, using the condition (b) of J , we can rewrite the energy (1) as

$$E(u) = \int_{\Omega} F(u) d\mathbf{x} + \frac{\varepsilon^2}{2} (\mathcal{L}u, u). \quad (4)$$

The nonlocal Cahn–Hilliard equation under consideration is the H^{-1} gradient flow with respect to the energy (4) with $F(u) = \frac{1}{4}(u^2 - 1)^2$, taking the form

$$u_t = \Delta(u^3 - u + \varepsilon^2 \mathcal{L}u), \quad (\mathbf{x}, t) \in \Omega_T, \quad (5)$$

where $T > 0$ is the terminal time, $\Omega_T = \Omega \times (0, T]$, and the unknown $u(\mathbf{x}, t)$ is subject to the initial condition $u(\mathbf{x}, 0) = u_0(\mathbf{x})$ for any $\mathbf{x} \in \Omega$ and the periodic boundary condition.

If J is further integrable, then $J * 1 = \int_{\Omega} J(\mathbf{x}) d\mathbf{x} > 0$ is a positive constant and

$$\mathcal{L}v = (J * 1)v - J * v, \quad (6)$$

where

$$(J * v)(\mathbf{x}) = \int_{\Omega} J(\mathbf{x} - \mathbf{y})v(\mathbf{y}) d\mathbf{y} = \int_{\Omega} J(\mathbf{y})v(\mathbf{x} - \mathbf{y}) d\mathbf{y}$$

is exactly the periodic convolution [24]. In this case, the equation (5) can be written as

$$u_t = \nabla \cdot (a(u) \nabla u) - \varepsilon^2 \Delta J * u,$$

where $a(u) = 3u^2 - 1 + \varepsilon^2 J * 1$ is referred as the diffusive mobility. If

$$\beta := \varepsilon^2 J * 1 - 1 > 0, \quad (7)$$

which gives $a(u) > 0$, then the equation (5) becomes diffusive and the solution becomes regular in time; otherwise, the solution may exhibit some singular behaviors. In order to ensure the successful computations of the FFT-based implementation without any breakdowns or unexpected oscillations, in this paper, we make some technical assumptions that there is no singularity existing in the solutions and the kernel J is integrable with the condition (7) satisfied.

2.2. Connection to the classic Cahn–Hilliard equation

The well-known classic Cahn–Hilliard equation [10] is given by

$$u_t = \Delta(u^3 - u - \varepsilon^2 \Delta u), \quad (8)$$

and the corresponding local energy functional by

$$E_{\text{local}}(u) = \int_{\Omega} \left(\frac{1}{4}(u^2 - 1)^2 + \frac{\varepsilon^2}{2} |\nabla u|^2 \right) d\mathbf{x}. \quad (9)$$

To illustrate the relationship between the local and nonlocal energies, we can approximate the interaction energy density using the Taylor (or Landau, as often in the physics literature) expansion [4,33], the periodicity of u and J , and the conditions (b)–(d) of J to find

$$\begin{aligned} \frac{\varepsilon^2}{4} \int_{\Omega} J(\mathbf{x} - \mathbf{y})(u(\mathbf{x}) - u(\mathbf{y}))^2 d\mathbf{y} &= \frac{\varepsilon^2}{4} \int_{\Omega} J(\mathbf{y})(u(\mathbf{x}) - u(\mathbf{x} + \mathbf{y}))^2 d\mathbf{y} \\ &\approx \frac{\varepsilon^2}{4} \int_{\Omega} J(\mathbf{y})|\mathbf{y}|^2 |\nabla u(\mathbf{x})|^2 d\mathbf{y} = \frac{\varepsilon^2}{2} |\nabla u(\mathbf{x})|^2. \end{aligned}$$

Therefore, the NCH equation (5) comes from replacing the second $-\Delta$ operator in the equation (8) by the nonlocal diffusion operator \mathcal{L} . A more rigorous derivation can be given by introducing a spatial interaction scale, say a nonlocal horizon parameter δ , in J and examining the limit of the nonlocal operator as $\delta \rightarrow 0$ to obtain the classic Laplacian operator, see for instance Proposition 3 given later and also additional related discussions in [9,16,31].

3. Spectral collocation approximations of spatial operators

In this section, we will present some notations and lemmas on the spectral collocation approximations for some spatial operators in the two-dimensional space with $\Omega = (-X, X) \times (-Y, Y)$.

Let N_x and N_y be two even numbers. The $N_x \times N_y$ mesh Ω_h of the domain Ω is a set of nodes (x_i, y_j) with $x_i = -X + ih_x$, $y_j = -Y + jh_y$, $1 \leq i \leq N_x$, $1 \leq j \leq N_y$, where $h_x = 2X/N_x$ and $h_y = 2Y/N_y$ are the uniform mesh sizes in each dimension. Let $h = \max\{h_x, h_y\}$. We define the index sets

$$\begin{aligned} S_h &= \{(i, j) \in \mathbb{Z}^2 \mid 1 \leq i \leq N_x, 1 \leq j \leq N_y\}, \\ \widehat{S}_h &= \left\{ (k, l) \in \mathbb{Z}^2 \mid -\frac{N_x}{2} + 1 \leq k \leq \frac{N_x}{2}, -\frac{N_y}{2} + 1 \leq l \leq \frac{N_y}{2} \right\}. \end{aligned}$$

All of the periodic grid functions defined on Ω_h are denoted by \mathcal{M}_h , that is,

$$\mathcal{M}_h = \{f : \Omega_h \rightarrow \mathbb{R} \mid f_{i+mN_x, j+nN_y} = f_{ij} \text{ for any } (i, j) \in S_h \text{ and } (m, n) \in \mathbb{Z}^2\}.$$

For any $f, g \in \mathcal{M}_h$ and $\mathbf{f} = (f^1, f^2)^T$, $\mathbf{g} = (g^1, g^2)^T \in \mathcal{M}_h \times \mathcal{M}_h$, the discrete L^2 inner product $\langle \cdot, \cdot \rangle$, discrete L^2 norm $\|\cdot\|_2$, and discrete L^∞ norm $\|\cdot\|_\infty$ are respectively defined by

$$\begin{aligned} \langle f, g \rangle &= h_x h_y \sum_{(i,j) \in S_h} f_{ij} g_{ij}, & \langle \mathbf{f}, \mathbf{g} \rangle &= h_x h_y \sum_{(i,j) \in S_h} (f_{ij}^1 g_{ij}^1 + f_{ij}^2 g_{ij}^2), \\ \|f\|_2 &= \sqrt{\langle f, f \rangle}, & \|\mathbf{f}\|_2 &= \sqrt{\langle \mathbf{f}, \mathbf{f} \rangle}, \\ \|f\|_\infty &= \max_{(i,j) \in S_h} |f_{ij}|, & \|\mathbf{f}\|_\infty &= \max_{(i,j) \in S_h} \sqrt{f_{ij}^1 + f_{ij}^2}. \end{aligned}$$

3.1. Discrete gradient, divergence and Laplace operators

For a function $f \in \mathcal{M}_h$, the 2D discrete Fourier transform $\hat{f} = Pf$ is defined componentwisely [37,41] by

$$\hat{f}_{kl} = \sum_{(i,j) \in S_h} f_{ij} \exp\left(-i\frac{k\pi}{X}x_i\right) \exp\left(-i\frac{l\pi}{Y}y_j\right), \quad (k, l) \in \widehat{S}_h. \quad (10)$$

The function f can be reconstructed via the corresponding inverse transform $f = P^{-1}\hat{f}$ with components given by

$$f_{ij} = \frac{1}{N_x N_y} \sum_{(k,l) \in \widehat{S}_h} \hat{f}_{kl} \exp\left(i\frac{k\pi}{X}x_i\right) \exp\left(i\frac{l\pi}{Y}y_j\right), \quad (i, j) \in S_h. \quad (11)$$

Let $\widehat{\mathcal{M}}_h = \{Pf \mid f \in \mathcal{M}_h\}$ and define the operators \widehat{D}_x and \widehat{D}_y on $\widehat{\mathcal{M}}_h$ as

$$(\widehat{D}_x \hat{f})_{kl} = \left(\frac{k\pi i}{X}\right) \hat{f}_{kl}, \quad (\widehat{D}_y \hat{f})_{kl} = \left(\frac{l\pi i}{Y}\right) \hat{f}_{kl}, \quad (k, l) \in \widehat{S}_h,$$

then the Fourier spectral approximations to the first and second order partial derivatives can be represented as

$$D_x = P^{-1} \widehat{D}_x P, \quad D_y = P^{-1} \widehat{D}_y P, \quad D_x^2 = P^{-1} \widehat{D}_x^2 P, \quad D_y^2 = P^{-1} \widehat{D}_y^2 P.$$

For any $f \in \mathcal{M}_h$ and $\mathbf{f} = (f^1, f^2)^T \in \mathcal{M}_h \times \mathcal{M}_h$, the discrete gradient, divergence and Laplace operators are given respectively by

$$\nabla_h f = \begin{pmatrix} D_x f \\ D_y f \end{pmatrix}, \quad \nabla_h \cdot \mathbf{f} = D_x f^1 + D_y f^2, \quad \Delta_h f = D_x^2 f + D_y^2 f.$$

It is easy to prove the following result:

Lemma 1. For any functions $f, g \in \mathcal{M}_h$ and $\mathbf{g} \in \mathcal{M}_h \times \mathcal{M}_h$, we have the discrete integration by parts formulas

$$\langle f, \nabla_h \cdot \mathbf{g} \rangle = -\langle \nabla_h f, \mathbf{g} \rangle, \quad \langle f, \Delta_h g \rangle = -\langle \nabla_h f, \nabla_h g \rangle = \langle \Delta_h f, g \rangle.$$

3.2. Discrete convolutions

To define the discrete convolutions, we consider the kernel function set

$$\mathcal{K}_h = \{\psi : \Omega_{h,0} \rightarrow \mathbb{R} \mid \psi_{i+mN_x, j+nN_y} = \psi_{ij} \text{ for any } (i, j) \in S_h \text{ and } (m, n) \in \mathbb{Z}^2\},$$

where $\Omega_{h,0} = \{(ih_x, jh_y) \mid (i, j) \in S_h\}$ is the mesh on the domain $(0, 2X) \times (0, 2Y)$. A discrete transform and its inversion of a function $\psi \in \mathcal{K}_h$ could be defined similarly via (10) and (11) by replacing x_i and y_j by ih_x and jh_y , respectively. Actually, \mathcal{K}_h is equivalent to \mathcal{M}_h due to the periodicity of their elements, and we consider the functions from \mathcal{K}_h as the kernels just for convenience of notations.

For any $\psi \in \mathcal{K}_h$ and $f \in \mathcal{M}_h$, the discrete convolution $\psi \circledast f \in \mathcal{M}_h$ is defined componentwisely by

$$(\psi \circledast f)_{ij} = h_x h_y \sum_{(m,n) \in S_h} \psi_{i-m, j-n} f_{mn}, \quad (i, j) \in S_h.$$

Then, direct calculations yield the following formula:

Lemma 2. For any functions $\psi \in \mathcal{K}_h$ and $f \in \mathcal{M}_h$, we have

$$(\psi \circledast f)_{ij} = \frac{h_x h_y}{N_x N_y} \sum_{(k,l) \in \widehat{S}_h} \hat{\psi}_{kl} \hat{f}_{kl} \exp\left(i\frac{k\pi}{X}x_i\right) \exp\left(i\frac{l\pi}{Y}y_j\right), \quad (i, j) \in S_h,$$

which means

$$\widehat{(\psi \circledast f)}_{kl} = h_x h_y \hat{\psi}_{kl} \hat{f}_{kl}, \quad (k, l) \in \widehat{S}_h.$$

Especially, by setting $f \equiv 1$ on Ω_h , we have

$$\psi \circledast 1 \equiv h_x h_y \hat{\psi}_{00} = h_x h_y \sum_{(m,n) \in S_h} \psi_{mn}.$$

3.3. Discrete nonlocal diffusion operator

Given an integrable kernel J satisfying the assumptions (a)–(c), we can define the action of the nonlocal operator \mathcal{L} on any grid function $f \in \mathcal{M}_h$ through the use of $\mathcal{L}_h = P^{-1} \hat{\mathcal{L}}_h P$ by

$$\hat{\mathcal{L}}_h \hat{f}_{kl} = \Lambda_{kl} \hat{f}_{kl}, \quad (k, l) \in \hat{S}_h,$$

where Λ_{kl} are the eigenvalues of \mathcal{L} given by (3). However, we see that except some special cases, one can hardly evaluate the integrals involved in (3) exactly, thus we need to find a more practical approach to define the discrete version of the nonlocal operator \mathcal{L} in space.

First, let us define the approximating nonlocal operator $\tilde{\mathcal{L}}$ on $L^2_{\text{per}}(\Omega)$ by

$$\tilde{\mathcal{L}} \exp\left(i \frac{k\pi}{X} x\right) \exp\left(i \frac{l\pi}{Y} y\right) = \lambda_{kl} \exp\left(i \frac{k\pi}{X} x\right) \exp\left(i \frac{l\pi}{Y} y\right), \quad (k, l) \in \mathbb{Z}^2,$$

where

$$\lambda_{kl} = h_x h_y \sum_{(i,j) \in S_h} J(x_i, y_j) \left(1 - \exp\left(-i \frac{k\pi}{X} x_i\right) \exp\left(-i \frac{l\pi}{Y} y_j\right) \right), \quad (12)$$

which is actually an approximation of (3) by using the periodic rectangular quadrature rule for the related integrals. Next, we define the discrete nonlocal diffusion operator \mathcal{L}_h on any grid function $f \in \mathcal{M}_h$ by $\mathcal{L}_h = P^{-1} \hat{\mathcal{L}}_h P$ with

$$\hat{\mathcal{L}}_h \hat{f}_{kl} = \lambda_{kl} \hat{f}_{kl}, \quad (k, l) \in \hat{S}_h,$$

where λ_{kl} 's are given by (12). Some important properties of \mathcal{L}_h are summarized below.

Lemma 3. *The operator \mathcal{L}_h has the following properties:*

- (i) *the eigenvalues of \mathcal{L}_h are $\lambda_{kl} = h_x h_y (\hat{J}_{00} - \hat{J}_{kl}) \geq 0$, $(k, l) \in \hat{S}_h$;*
- (ii) *\mathcal{L}_h commutes with Δ_h and is self-adjoint and positive semi-definite;*
- (iii) *for any $f \in \mathcal{M}_h$, we have $\mathcal{L}_h f = (J \circledast 1) f - J \circledast f$.*

Proof. Using the notations of the discrete Fourier transforms, we can express (12) as

$$\lambda_{kl} = h_x h_y (\hat{J}_{00} - \hat{J}_{kl}).$$

On the other hand, since J is real and even, we know that \hat{J}_{kl} and λ_{kl} are also real and even with respect to $(k, l) \in \hat{S}_h$. So we can rewrite (12) as

$$\lambda_{kl} = h_x h_y \sum_{(i,j) \in S_h} J(x_i, y_j) \left(1 - \cos\left(\frac{k\pi}{X} x_i + \frac{l\pi}{Y} y_j\right) \right).$$

Since $J_{ij} \geq 0$ due to the assumption (a), we obtain $\lambda_{kl} \geq 0$, which implies directly the positive semi-definiteness of \mathcal{L}_h .

We know from the definition of the discrete operator \mathcal{L}_h that both \mathcal{L}_h and Δ_h can be diagonalized by the transform P , which implies that \mathcal{L}_h commutes with Δ_h . The property (iii) is the direct consequence of using Lemma 2. \square

Remark. In Lemma 3, the property (i) implies that the eigenvalues $\{\lambda_{kl}\}$ can be computed efficiently via the FFT technique, and the property (iii) gives us an equivalent definition of \mathcal{L}_h , which is exactly the discrete version of (6).

4. Stabilized linear semi-implicit schemes

In this section, we construct and analyze first and second order (in time) stabilized semi-implicit fully discrete schemes for solving the NCH equation (5), respectively. The spectral collocation approximations defined in Section 3 are used for spatial discretization. Given a positive integer N_t , let us partition the time interval $[0, T]$ by $\{t_n = n\tau\}_{n=0}^{N_t}$ with the time step size $\tau = T/N_t$.

4.1. First order scheme

The first order stabilized linear semi-implicit (SSI1) scheme of the NCH equation (5) is constructed as follows: for $0 \leq n \leq N_t - 1$, find $u_h^{n+1} = (u_{ij}^{n+1}) \in \mathcal{M}_h$ such that

$$u_h^{n+1} - u_h^n = \tau \Delta_h w_h^{n+1}, \quad (13a)$$

$$w_h^{n+1} = (\varepsilon^2 \mathcal{L}_h + A \mathcal{I}_h) u_h^{n+1} + (u_h^n)^3 - (A + 1) u_h^n, \quad (13b)$$

with $u_h^0 = (u_{ij}^0) \in \mathcal{M}_h$ given by the initial data, $A > 0$ a stabilization constant, and \mathcal{I}_h the identity operator. The SSI1 scheme (13) is obtained by treating the nonlocal diffusion term in (5) implicitly and the nonlinear potential term explicitly, and adding a stabilizing term $A \Delta_h (u_h^{n+1} - u_h^n)$ for the sake of stability. The following proposition gives us the unique solvability of the scheme (13) and the property of mass conservation in the discrete version.

Proposition 1 (Solvability and mass conservation of the SSI1 scheme). *For any $\tau > 0$, the SSI1 scheme (13) has a unique solution $u_h^{n+1} \in \mathcal{M}_h$ for given $u_h^n \in \mathcal{M}_h$. Moreover, $\langle u_h^{n+1} - u_h^n, 1 \rangle = 0$ for $0 \leq n \leq N_t - 1$.*

Proof. The SSI1 scheme (13) could be rewritten as

$$[\mathcal{I}_h - \tau \Delta_h (\varepsilon^2 \mathcal{L}_h + A \mathcal{I}_h)] u_h^{n+1} = u_h^n + \tau \Delta_h [(u_h^n)^3 - (A + 1) u_h^n]. \quad (14)$$

Since \mathcal{L}_h commutes with Δ_h , the unique solvability is obvious due to the positive definiteness of $\mathcal{I}_h - \tau \Delta_h (\varepsilon^2 \mathcal{L}_h + A \mathcal{I}_h)$. Taking the discrete L^2 inner product of (13a) with $v \equiv 1$ gives us $\langle u_h^{n+1} - u_h^n, 1 \rangle = 0$. \square

According to the definitions of discrete spatial operators presented in the previous section, the unique solution to (14) (i.e., (13)) can be computed in the frequency space via

$$\hat{u}_{kl}^{n+1} = \frac{\hat{u}_{kl}^n - \tau (k^2 + l^2) (\hat{q}_{kl}^n - (A + 1) \hat{u}_{kl}^n)}{1 + \tau (k^2 + l^2) (\varepsilon^2 \lambda_{kl} + A)},$$

with $q_h^n = (u_h^n)^3$ and $\{\lambda_{kl}\}$ being the eigenvalues of \mathcal{L}_h given by (12).

Now we consider the energy stability of the SSI1 scheme (13). Define a discrete version of the energy (4) as

$$E_h(u_h) = \frac{1}{4} \| (u_h)^2 \|_2^2 - \frac{1}{2} \| u_h \|_2^2 + \frac{1}{4} |\Omega| + \frac{\varepsilon^2}{2} \langle \mathcal{L}_h u_h, u_h \rangle, \quad \forall u_h \in \mathcal{M}_h, \quad (15)$$

then we have the following result for the SSI1 scheme:

Theorem 1 (Energy stability of the SSI1 scheme). *For any $\tau > 0$, it holds that*

$$E_h(u_h^{n+1}) + \tau \|\nabla_h w_h^{n+1}\|_2^2 + R_h(u_h^n, u_h^{n+1}) = E_h(u_h^n), \quad 0 \leq n \leq N_t - 1, \quad (16)$$

where

$$R_h(u_h^n, u_h^{n+1}) = \frac{1}{2} \langle \mathcal{L}_h (u_h^{n+1} - u_h^n), u_h^{n+1} - u_h^n \rangle + \langle A - \frac{1}{2} (u_h^n)^2 - \frac{1}{4} (u_h^{n+1} + u_h^n)^2 + \frac{1}{2}, (u_h^{n+1} - u_h^n)^2 \rangle.$$

Moreover, the energy is nonincreasing for any $\tau > 0$, i.e., $E_h(u_h^{n+1}) \leq E_h(u_h^n)$, provided that the constant A satisfies

$$A \geq \max_{(i,j) \in S_h} \left\{ \frac{1}{2} (u_{ij}^n)^2 + \frac{1}{4} (u_{ij}^{n+1} + u_{ij}^n)^2 - \frac{1}{2} \right\}. \quad (17)$$

Proof. Taking the discrete L^2 inner product of (13a) with w_h^{n+1} leads to

$$\langle u_h^{n+1} - u_h^n, w_h^{n+1} \rangle = \tau \langle \Delta_h w_h^{n+1}, w_h^{n+1} \rangle = -\tau \|\nabla_h w_h^{n+1}\|_2^2. \quad (18)$$

Taking the discrete L^2 inner product of (13b) with $u_h^{n+1} - u_h^n$ leads to

$$\langle w_h^{n+1}, u_h^{n+1} - u_h^n \rangle = \varepsilon^2 \langle \mathcal{L}_h u_h^{n+1}, u_h^{n+1} - u_h^n \rangle + \langle (u_h^n)^3 - u_h^n, u_h^{n+1} - u_h^n \rangle + A \|u_h^{n+1} - u_h^n\|_2^2.$$

Using the identity $\mathbf{a} \cdot (\mathbf{a} - \mathbf{b}) = \frac{1}{2} |\mathbf{a}|^2 - \frac{1}{2} |\mathbf{b}|^2 + \frac{1}{2} |\mathbf{a} - \mathbf{b}|^2$, we have

$$\langle \mathcal{L}_h u_h^{n+1}, u_h^{n+1} - u_h^n \rangle = \frac{1}{2} \langle \mathcal{L}_h u_h^{n+1}, u_h^{n+1} \rangle - \frac{1}{2} \langle \mathcal{L}_h u_h^n, u_h^n \rangle + \frac{1}{2} \langle \mathcal{L}_h (u_h^{n+1} - u_h^n), u_h^{n+1} - u_h^n \rangle.$$

By some simple calculations, we can find that

$$\begin{aligned} \langle (u_h^n)^3 - u_h^n, u_h^{n+1} - u_h^n \rangle &= \frac{1}{4} \|(u_h^{n+1})^2\|_2^2 - \frac{1}{4} \|(u_h^n)^2\|_2^2 - \frac{1}{2} \|u_h^{n+1}\|_2^2 + \frac{1}{2} \|u_h^n\|_2^2 \\ &\quad - \left\langle \frac{1}{2}(u_h^n)^2 + \frac{1}{4}(u_h^{n+1} + u_h^n)^2 - \frac{1}{2}, (u_h^{n+1} - u_h^n)^2 \right\rangle. \end{aligned}$$

Then, we obtain

$$\begin{aligned} \langle w_h^{n+1}, u_h^{n+1} - u_h^n \rangle &= \frac{\varepsilon^2}{2} \langle \mathcal{L}_h u_h^{n+1}, u_h^{n+1} \rangle - \frac{\varepsilon^2}{2} \langle \mathcal{L}_h u_h^n, u_h^n \rangle + \frac{\varepsilon^2}{2} \langle \mathcal{L}_h (u_h^{n+1} - u_h^n), u_h^{n+1} - u_h^n \rangle \\ &\quad + \frac{1}{4} \|(u_h^{n+1})^2\|_2^2 - \frac{1}{4} \|(u_h^n)^2\|_2^2 - \frac{1}{2} \|u_h^{n+1}\|_2^2 + \frac{1}{2} \|u_h^n\|_2^2 \\ &\quad + \langle A - \frac{1}{2}(u_h^n)^2 - \frac{1}{4}(u_h^{n+1} + u_h^n)^2 + \frac{1}{2}, (u_h^{n+1} - u_h^n)^2 \rangle \\ &= E_h(u_h^{n+1}) - E_h(u_h^n) + R_h(u_h^n, u_h^{n+1}). \end{aligned} \quad (19)$$

Combining (18) and (19), we obtain (16). Since \mathcal{L}_h is positive semi-definite, we have

$$R_h(u_h^n, u_h^{n+1}) \geq \langle A - \frac{1}{2}(u_h^n)^2 - \frac{1}{4}(u_h^{n+1} + u_h^n)^2 + \frac{1}{2}, (u_h^{n+1} - u_h^n)^2 \rangle.$$

Under the condition (17), we have $R_h(u_h^n, u_h^{n+1}) \geq 0$. \square

Remark. The condition (17) implies an assumption on the uniform discrete L^∞ boundness of the numerical solution, while such an assumption is necessary to show the energy stability, as is claimed in [25]. Another way to keep the stability, adopted in [38], is to assume the Lipschitz continuity of the derivative of the potential F , namely, $|F''(u)| \leq L$ for some $L > 0$. For the case with the quartic potential, such two assumptions are equivalent to each other and inevitable in the analysis for the stability and convergence of the stabilized schemes. Though there are some new techniques [29,30] removing such assumptions for the case of local Cahn–Hilliard model, whether they could be applied on the nonlocal models is still open. Fortunately, in most practical simulations, the computed solutions are always bounded uniformly in the space-time mesh, so our theoretical results are still valid in this version.

4.2. Second order scheme

The second order stabilized linear semi-implicit (SSI2) scheme for the NCH equation (5) is constructed as follows: for $1 \leq n \leq N_t - 1$, find $u_h^{n+1} = (u_{ij}^{n+1}) \in \mathcal{M}_h$ such that

$$u_h^{n+1} - u_h^n = \tau \Delta_h w^{n+\frac{1}{2}}, \quad (20a)$$

$$w_h^{n+\frac{1}{2}} = (\varepsilon^2 \mathcal{L}_h + A \mathcal{I}_h) \left(\frac{3}{4} u_h^{n+1} + \frac{1}{4} u_h^{n-1} \right) + \frac{3}{2} (u_h^n)^3 - \frac{1}{2} (u_h^{n-1})^3 - (A+1) \left(\frac{3}{2} u_h^n - \frac{1}{2} u_h^{n-1} \right), \quad (20b)$$

with $u_h^0 = (u_{ij}^0)$ given by the initial data and $u_h^1 = (u_{ij}^1)$ computed by the SSI1 scheme (13) with $n = 0$. The SSI2 scheme (20) is equivalent to

$$\begin{aligned} \left[\mathcal{I}_h - \frac{3\tau}{4} \Delta_h (\varepsilon^2 \mathcal{L}_h + A \mathcal{I}_h) \right] u_h^{n+1} &= u_h^n + \frac{\tau}{4} \Delta_h (\varepsilon^2 \mathcal{L}_h + A \mathcal{I}_h) u_h^{n-1} \\ &\quad + \tau \Delta_h \left[\frac{3}{2} (u_h^n)^3 - \frac{1}{2} (u_h^{n-1})^3 - (A+1) \left(\frac{3}{2} u_h^n - \frac{1}{2} u_h^{n-1} \right) \right], \end{aligned}$$

which can be solved efficiently by using the FFT technique and updating in the frequency space via

$$\hat{u}_{kl}^{n+1} = \frac{\hat{u}_{kl}^n - \tau (k^2 + l^2) [\frac{1}{4} (\varepsilon^2 \lambda_{kl} + A) \hat{u}_{kl}^{n-1} + (\frac{3}{2} \hat{q}_{kl}^n - \frac{1}{2} \hat{q}_{kl}^{n-1}) - (A+1) (\frac{3}{2} \hat{u}_{kl}^n - \frac{1}{2} \hat{u}_{kl}^{n-1})]}{1 + \frac{3\tau}{4} (k^2 + l^2) (\varepsilon^2 \lambda_{kl} + A)},$$

with $q_h^n = (u_h^n)^3$, $q_h^{n-1} = (u_h^{n-1})^3$ and $\{\lambda_{kl}\}$ given by (12). There is no essential difference between the proofs of the unique solvability for the SSI1 and SSI2 schemes, so we present the following result without proof.

Proposition 2 (Solvability and mass conservation of the SSI2 scheme). For any $\tau > 0$, the SSI2 scheme (20) has a unique solution $u_h^{n+1} \in \mathcal{M}_h$ for given u_h^{n-1} , $u_h^n \in \mathcal{M}_h$. Moreover, $\langle u_h^{n+1} - u_h^n, 1 \rangle = 0$ for $0 \leq n \leq N_t - 1$.

For $1 \leq n \leq N_t$, now let us define a modified discrete energy functional as

$$\mathcal{E}_h(u_h^n, u_h^{n-1}) = E_h(u_h^n) + \frac{\varepsilon^2}{8} \langle \mathcal{L}_h(u_h^n - u_h^{n-1}), u_h^n - u_h^{n-1} \rangle + \frac{3A + 2}{8} \|u_h^n - u_h^{n-1}\|_2^2,$$

which is clearly a second order approximation of the original discrete energy $E_h(u_h^n)$ defined in (15).

Theorem 2 (Energy stability of the SSI2 scheme). *For any $\tau > 0$, we have*

$$\mathcal{E}_h(u_h^{n+1}, u_h^n) \leq \mathcal{E}_h(u_h^n, u_h^{n-1}) + A \|u_h^{n+1} - u_h^n\|_2^2, \quad 1 \leq n \leq N_t - 1,$$

provided that the constant A satisfies

$$A \geq \max \left\{ \frac{1}{3} \max_{(i,j) \in S_h} \{(u_{ij}^n)^2 + (u_{ij}^{n-1})^2 + (u_{ij}^n + u_{ij}^{n-1})^2\} - 2, \max_{(i,j) \in S_h} \left\{ \frac{1}{2} (u_{ij}^n)^2 + \frac{1}{4} (u_{ij}^{n+1} + u_{ij}^n)^2 \right\} \right\}. \quad (21)$$

Proof. Taking the discrete L^2 inner product of (20a) with $w^{n+\frac{1}{2}}$, we have

$$\langle u_h^{n+1} - u_h^n, w^{n+\frac{1}{2}} \rangle = \tau \langle \Delta_h w^{n+\frac{1}{2}}, w^{n+\frac{1}{2}} \rangle = -\tau \|\nabla_h w^{n+\frac{1}{2}}\|_2^2 \leq 0. \quad (22)$$

Taking the discrete L^2 inner product of (20b) with $u_h^{n+1} - u_h^n$, we obtain

$$\begin{aligned} \langle w^{n+\frac{1}{2}}, u_h^{n+1} - u_h^n \rangle &= \left\langle \left(\varepsilon^2 \mathcal{L}_h + A \mathcal{I}_h \right) \left(\frac{3}{4} u_h^{n+1} + \frac{1}{4} u_h^{n-1} \right), u_h^{n+1} - u_h^n \right\rangle \\ &\quad + \frac{1}{2} \langle (u_h^n)^3 - (u_h^{n-1})^3, u_h^{n+1} - u_h^n \rangle - \frac{A+1}{2} \langle 3u_h^n - u_h^{n-1}, u_h^{n+1} - u_h^n \rangle \\ &= \varepsilon^2 \left\langle \mathcal{L}_h \left(\frac{3}{4} u_h^{n+1} + \frac{1}{4} u_h^{n-1} \right), u_h^{n+1} - u_h^n \right\rangle \\ &\quad + \langle (u_h^n)^3 - u_h^n, u_h^{n+1} - u_h^n \rangle - \frac{1}{2} \langle u_h^n - u_h^{n-1}, u_h^{n+1} - u_h^n \rangle \\ &\quad + \frac{1}{2} \langle (u_h^n)^3 - (u_h^{n-1})^3, u_h^{n+1} - u_h^n \rangle + \frac{3A}{4} \langle u_h^{n+1} - 2u_h^n + u_h^{n-1}, u_h^{n+1} - u_h^n \rangle, \end{aligned}$$

where the second term in the right-hand side of the last equality could be derived identically to the proof of Theorem 1 as follows:

$$\begin{aligned} \langle (u_h^n)^3 - u_h^n, u_h^{n+1} - u_h^n \rangle &= \frac{1}{4} \|(u_h^{n+1})^2\|_2^2 - \frac{1}{4} \|(u_h^n)^2\|_2^2 - \frac{1}{2} \|u_h^{n+1}\|_2^2 + \frac{1}{2} \|u_h^n\|_2^2 \\ &\quad - \langle \frac{1}{2} (u_h^n)^2 + \frac{1}{4} (u_h^{n+1} + u_h^n)^2, (u_h^{n+1} - u_h^n)^2 \rangle + \frac{1}{2} \|u_h^{n+1} - u_h^n\|_2^2. \end{aligned}$$

By using the identity

$$\left(\frac{3}{4} \mathbf{a} + \frac{1}{4} \mathbf{c} \right) \cdot (\mathbf{a} - \mathbf{b}) = \frac{1}{2} |\mathbf{a}|^2 - \frac{1}{2} |\mathbf{b}|^2 + \frac{1}{8} |\mathbf{a} - \mathbf{b}|^2 - \frac{1}{8} |\mathbf{b} - \mathbf{c}|^2 + \frac{1}{8} |\mathbf{a} - 2\mathbf{b} + \mathbf{c}|^2,$$

we get

$$\begin{aligned} \left\langle \mathcal{L}_h \left(\frac{3}{4} u_h^{n+1} + \frac{1}{4} u_h^{n-1} \right), u_h^{n+1} - u_h^n \right\rangle &= \frac{1}{2} \langle \mathcal{L}_h u_h^{n+1}, u_h^{n+1} \rangle - \frac{1}{2} \langle \mathcal{L}_h u_h^n, u_h^n \rangle + \frac{1}{8} \langle \mathcal{L}_h (u_h^{n+1} - u_h^n), u_h^{n+1} - u_h^n \rangle \\ &\quad - \frac{1}{8} \langle \mathcal{L}_h (u_h^n - u_h^{n-1}), u_h^n - u_h^{n-1} \rangle \\ &\quad + \frac{1}{8} \langle \mathcal{L}_h (u_h^{n+1} - 2u_h^n + u_h^{n-1}), u_h^{n+1} - 2u_h^n + u_h^{n-1} \rangle. \end{aligned}$$

Using the identity $\mathbf{a} \cdot (\mathbf{a} - \mathbf{b}) = \frac{1}{2} |\mathbf{a}|^2 - \frac{1}{2} |\mathbf{b}|^2 + \frac{1}{2} |\mathbf{a} - \mathbf{b}|^2$, we then obtain by setting $\mathbf{a} = u_h^{n+1} - u_h^n$ and $\mathbf{b} = u_h^n - u_h^{n-1}$ that

$$\langle u_h^{n+1} - 2u_h^n + u_h^{n-1}, u_h^{n+1} - u_h^n \rangle = \frac{1}{2} \|u_h^{n+1} - u_h^n\|_2^2 - \frac{1}{2} \|u_h^n - u_h^{n-1}\|_2^2 + \frac{1}{2} \|u_h^{n+1} - 2u_h^n + u_h^{n-1}\|_2^2$$

and by setting $\mathbf{a} = u_h^{n+1} - u_h^n$ and $\mathbf{b} = u_h^{n+1} - 2u_h^n + u_h^{n-1}$ that

$$\langle u_h^n - u_h^{n-1}, u_h^{n+1} - u_h^n \rangle = \frac{1}{2} \|u_h^{n+1} - u_h^n\|_2^2 + \frac{1}{2} \|u_h^n - u_h^{n-1}\|_2^2 - \frac{1}{2} \|u_h^{n+1} - 2u_h^n + u_h^{n-1}\|_2^2.$$

Consequently we further obtain

$$\begin{aligned}
\langle w^{n+\frac{1}{2}}, u_h^{n+1} - u_h^n \rangle &= \frac{\varepsilon^2}{2} \langle \mathcal{L}_h u_h^{n+1}, u_h^{n+1} \rangle - \frac{\varepsilon^2}{2} \langle \mathcal{L}_h u_h^n, u_h^n \rangle + \frac{\varepsilon^2}{8} \langle \mathcal{L}_h(u_h^{n+1} - u_h^n), u_h^{n+1} - u_h^n \rangle \\
&\quad - \frac{\varepsilon^2}{8} \langle \mathcal{L}_h(u_h^n - u_h^{n-1}), u_h^n - u_h^{n-1} \rangle + \frac{\varepsilon^2}{8} \langle \mathcal{L}_h(u_h^{n+1} - 2u_h^n + u_h^{n-1}), u_h^{n+1} - 2u_h^n + u_h^{n-1} \rangle \\
&\quad + \frac{1}{4} \|(u_h^{n+1})^2\|_2^2 - \frac{1}{4} \|(u_h^n)^2\|_2^2 - \frac{1}{2} \|u_h^{n+1}\|_2^2 + \frac{1}{2} \|u_h^n\|_2^2 \\
&\quad - \langle \frac{1}{2}(u_h^n)^2 + \frac{1}{4}(u_h^{n+1} + u_h^n)^2, (u_h^{n+1} - u_h^n)^2 \rangle + \frac{1}{2} \|u_h^{n+1} - u_h^n\|_2^2 \\
&\quad - \frac{1}{4} \|u_h^{n+1} - u_h^n\|_2^2 - \frac{1}{4} \|u_h^n - u_h^{n-1}\|_2^2 + \frac{1}{4} \|u_h^{n+1} - 2u_h^n + u_h^{n-1}\|_2^2 \\
&\quad + \frac{1}{2} \langle (u_h^n)^3 - (u_h^{n-1})^3, u_h^{n+1} - u_h^n \rangle \\
&\quad + \frac{3A}{8} \|u_h^{n+1} - u_h^n\|_2^2 - \frac{3A}{8} \|u_h^n - u_h^{n-1}\|_2^2 + \frac{3A}{8} \|u_h^{n+1} - 2u_h^n + u_h^{n-1}\|_2^2 \\
&= \left[E_h(u_h^{n+1}) + \frac{\varepsilon^2}{8} \langle \mathcal{L}_h(u_h^{n+1} - u_h^n), u_h^{n+1} - u_h^n \rangle + \frac{3A+2}{8} \|u_h^{n+1} - u_h^n\|_2^2 \right] \\
&\quad - \left[E_h(u_h^n) + \frac{\varepsilon^2}{8} \langle \mathcal{L}_h(u_h^n - u_h^{n-1}), u_h^n - u_h^{n-1} \rangle + \frac{3A+2}{8} \|u_h^n - u_h^{n-1}\|_2^2 \right] \\
&\quad + \left[\frac{\varepsilon^2}{8} \langle \mathcal{L}_h(u_h^{n+1} - 2u_h^n + u_h^{n-1}), u_h^{n+1} - 2u_h^n + u_h^{n-1} \rangle + \frac{3A+2}{8} \|u_h^{n+1} - 2u_h^n + u_h^{n-1}\|_2^2 \right. \\
&\quad \left. - \langle \frac{1}{2}(u_h^n)^2 + \frac{1}{4}(u_h^{n+1} + u_h^n)^2, (u_h^{n+1} - u_h^n)^2 \rangle + \frac{1}{2} \langle (u_h^n)^3 - (u_h^{n-1})^3, u_h^{n+1} - u_h^n \rangle \right],
\end{aligned}$$

thus we have

$$\langle w^{n+\frac{1}{2}}, u_h^{n+1} - u_h^n \rangle = \mathcal{E}_h(u_h^{n+1}, u_h^n) - \mathcal{E}_h(u_h^n, u_h^{n-1}) + R_h(u_h^{n-1}, u_h^n, u_h^{n+1}) \quad (23)$$

with

$$\begin{aligned}
R_h(u_h^{n-1}, u_h^n, u_h^{n+1}) &\geq \frac{3A+2}{8} \|u_h^{n+1} - 2u_h^n + u_h^{n-1}\|_2^2 + \frac{1}{2} \langle (u_h^n)^3 - (u_h^{n-1})^3, u_h^{n+1} - u_h^n \rangle \\
&\quad - \langle \frac{1}{2}(u_h^n)^2 + \frac{1}{4}(u_h^{n+1} + u_h^n)^2, (u_h^{n+1} - u_h^n)^2 \rangle.
\end{aligned}$$

Notice that

$$\begin{aligned}
\langle (u_h^n)^3 - (u_h^{n-1})^3, u_h^{n+1} - u_h^n \rangle &= \langle (u_h^n)^2 + (u_h^{n-1})^2 + u_h^n u_h^{n-1}, (u_h^n - u_h^{n-1})(u_h^{n+1} - u_h^n) \rangle \\
&= \frac{1}{4} \langle (u_h^n)^2 + (u_h^{n-1})^2 + (u_h^n + u_h^{n-1})^2, (u_h^{n+1} - u_h^n)^2 + (u_h^n - u_h^{n-1})^2 \\
&\quad - (u_h^{n+1} - 2u_h^n + u_h^{n-1})^2 \rangle,
\end{aligned}$$

then, under the condition (21), we further have

$$\begin{aligned}
R_h(u_h^{n-1}, u_h^n, u_h^{n+1}) &\geq \frac{3A+2}{8} \|u_h^{n+1} - 2u_h^n + u_h^{n-1}\|_2^2 - \langle \frac{1}{2}(u_h^n)^2 + \frac{1}{4}(u_h^{n+1} + u_h^n)^2, (u_h^{n+1} - u_h^n)^2 \rangle \\
&\quad + \frac{1}{8} \langle (u_h^n)^2 + (u_h^{n-1})^2 + (u_h^n + u_h^{n-1})^2, (u_h^{n+1} - u_h^n)^2 + (u_h^n - u_h^{n-1})^2 \rangle \\
&\quad - \frac{1}{8} \langle (u_h^n)^2 + (u_h^{n-1})^2 + (u_h^n + u_h^{n-1})^2, (u_h^{n+1} - 2u_h^n + u_h^{n-1})^2 \rangle \\
&\geq \left(\frac{3A+2}{8} - \frac{1}{8} \langle (u_h^n)^2 + (u_h^{n-1})^2 + (u_h^n + u_h^{n-1})^2, (u_h^{n+1} - 2u_h^n + u_h^{n-1})^2 \rangle \right. \\
&\quad \left. - \langle \frac{1}{2}(u_h^n)^2 + \frac{1}{4}(u_h^{n+1} + u_h^n)^2, (u_h^{n+1} - u_h^n)^2 \rangle \right. \\
&\quad \left. - \langle \frac{1}{2}(u_h^n)^2 + \frac{1}{4}(u_h^{n+1} + u_h^n)^2, (u_h^{n+1} - u_h^n)^2 \rangle \right. \\
&\geq -A \|u_h^{n+1} - u_h^n\|_2^2.
\end{aligned}$$

The proof is then completed by using (22) and (23) with the above inequality. \square

5. Numerical experiments

In this section, we use the proposed time-stepping schemes to simulate the NCH equation (5) equipped with the Gaussian kernel J_δ given by (24) below. We first carry out some numerical experiments to test the temporal convergence rates of the SSI1 and SSI2 schemes. Then we select various (ε, δ) values to investigate shapes of the interfaces between phases in the steady states. Finally we perform some simulations to study the coarsening dynamics of the phase transition in the long time evolution.

The family of smooth kernels, given by the Gauss-type functions, take on the form of

$$J_\delta(\mathbf{x}) = \frac{4}{\pi^{d/2} \delta^{d+2}} e^{-\frac{|\mathbf{x}|^2}{\delta^2}}, \quad \mathbf{x} \in \mathbb{R}^d, \quad \delta > 0, \quad (24)$$

and satisfy

$$C_\delta := \int_{\mathbb{R}^d} J_\delta(\mathbf{x}) d\mathbf{x} = \frac{4}{\delta^2}$$

and

$$\int_{\mathbb{R}^d} J_\delta(\mathbf{x}) |\mathbf{x}|^2 d\mathbf{x} = 2d. \quad (25)$$

Since J_δ decays exponentially as $|\mathbf{x}| \rightarrow \infty$, we are allowed to regard J_δ as a function with a compact support in the finite domain Ω when the size of Ω is large enough compared with δ . Thus, J_δ can be further periodically extended to \mathbb{R}^d with respect to Ω . Correspondingly, we denote by \mathcal{L}_δ the nonlocal diffusion operator obtained by replacing J by the Ω -periodic version of J_δ in (2).

Proposition 3. For any $v \in C^\infty(\Omega)$ and any $\mathbf{x} \in \Omega$, $\mathcal{L}_\delta v(\mathbf{x}) \rightarrow -\Delta v(\mathbf{x})$ as $\delta \rightarrow 0$.

As a consequence of (25), Proposition 3 is often featured in the analysis of nonlocal diffusion problems (e.g., [15,40]). It tells us that the NCH equation (5) equipped with the Gaussian kernel (24) converges to the local Cahn–Hilliard equation (8) as δ goes to zero. One may also obtain the consistency of \mathcal{L}_δ and $-\Delta$ for functions that are not sufficiently smooth, see related discussions in [9,16,31]. The following result is similar in spirit to the Proposition 6 given in [16].

Proposition 4. The steady state solution u^* of the NCH equation (5) equipped with the Gaussian kernel (24) is continuous if $\delta \leq 2\varepsilon$.

Proof. Since $\mathcal{L}_\delta v = C_\delta v - J_\delta * v$, the steady state u^* satisfies

$$\Delta[(u^*)^3 + (\varepsilon^2 C_\delta - 1)u^* - \varepsilon^2 J_\delta * u^*] = 0.$$

According to the Liouville's theorem, i.e., every bounded harmonic function must be constant, we obtain

$$(u^*)^3 + (\varepsilon^2 C_\delta - 1)u^* - \varepsilon^2 J_\delta * u^* = C,$$

or equivalently,

$$(u^*)^3 + (\varepsilon^2 C_\delta - 1)u^* = \varepsilon^2 J_\delta * u^* + C.$$

Since J_δ is smooth, the right-hand-side of above is a continuous function in \mathbb{R}^d . Denote by $\mathcal{N}(u^*)$ the left-hand-side. We know that, if $\varepsilon^2 C_\delta - 1 \geq 0$, the continuous mapping $\mathcal{N} : \mathbb{R} \rightarrow \mathbb{R}$ is increasing strictly, which implies the existence of the continuous inverse of \mathcal{N} . Therefore, $u^* = \mathcal{N}^{-1}(\varepsilon^2 J_\delta * u^* + C)$ is continuous in \mathbb{R}^d . \square

Remark. The continuity condition $\delta \leq 2\varepsilon$ is equivalent to $\beta \geq 0$.

5.1. Convergence rates in time

Example 1. We consider the evolutions governed by the NCH equation (5) equipped with the Gaussian kernel J_δ in the periodic cell $\Omega = (-1, 1) \times (-1, 1)$ up to the time $T = 0.05$. The initial condition is set to be

$$u_0(x, y) = 0.5 \sin \pi x \sin \pi y + 0.1.$$

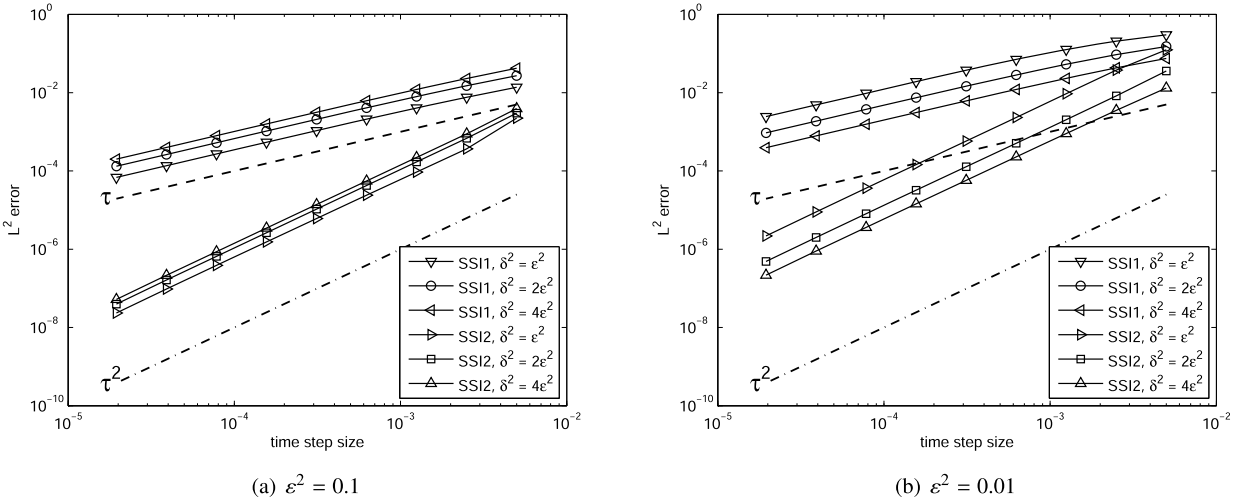


Fig. 1. Convergence rates in time of the SSI1 and SSI2 schemes in Example 1.

For the spatial discretization, we adopt the Fourier spectral collocation method on the uniform $N \times N$ mesh and choose N sufficiently large so that the errors caused by the spatial approximation could be ignored. Based on the numerical tests, we find that it is sufficient to fix $N = 1024$, and perform the numerical simulations using the time step sizes $\tau = 2^{-k}\Delta$, $k = 0, 1, 2, \dots, 8$ with $\Delta = 0.005$. The approximate solution obtained by the SSI2 scheme with $\tau = 2^{-8}\Delta/5$ is taken as the benchmark solution for computing errors. To meet the requirements of the stability, we set $A = 2$ and $A = 3$ for the SSI1 and SSI2 schemes, respectively.

Fig. 1 shows the discrete L^2 errors of the numerical solutions coming from the cases $\varepsilon^2 = 0.1$ and $\varepsilon^2 = 0.01$ with $\delta^2 = \varepsilon^2$, $\delta^2 = 2\varepsilon^2$, and $\delta^2 = 4\varepsilon^2$. We see from the figure that the first and second order convergence rates of the SSI1 and SSI2 schemes, respectively, are obvious and independent on the values of ε .

5.2. Interfaces in the steady states

Now we investigate the shapes of the interfaces formed in the steady states of the phase transitions governed by the NCH equation (5) with the Gaussian kernel under various ε and δ . The parameter ε is known to describe the interface width, as in the case of classic phase field models, and the parameter δ , usually called the horizon parameter for the nonlocal diffusion operator \mathcal{L}_δ , characterizes the range of nonlocal interactions [15]. In order to observe the interfacial motion more closely, we focus on the one-dimensional case.

Example 2. We choose $\Omega = (-1, 1)$ and $u_0(x) = 0.1(\sin 2\pi x + \sin 3\pi x)$, and adopt the SSI2 scheme with $A = 3$, $N = 8192$ and $\tau = 0.0001$ to simulate the phase transition till the steady state.

Some numerical results are presented in Fig. 2, where $\delta^2 = 0.01$, and ε is chosen as 0.25, 0.2, 0.15, 0.1, 0.08, and 0.06, and all of them satisfy the continuity condition stated in Proposition 4. The energy stability of the SSI2 scheme can be seen in the last column of the figure. For the cases $\varepsilon = 0.25$, 0.2, and 0.15, the graphs in the first row present the steady states and energy evolutions, where all the energies remain unchanged after $t = 5$, indicating that the steady states are reached for all cases. Similarly, the configurations and energies for other three cases are given in the second row, and we view the states at $t = 100$ as the steady ones. It is observed that the smaller ε is, the longer time is needed for the evolution to reach the steady state with sharper interfaces. Such phenomena are similar to those for the local Cahn–Hilliard equation [18].

In Fig. 3, we fix $\varepsilon = 0.1$, and choose δ^2 as 0.04, 0.03, 0.02, and 0.01. For comparison, we also simulate the local Cahn–Hilliard equation (8) with $\varepsilon = 0.1$. The energy stability of the SSI2 scheme in all cases can be seen in Fig. 3(c) and the steady states are already obtained for all cases at the final time $t = 10$. We observe from Fig. 3(a) and Fig. 3(b) that the shapes of the interfaces depend highly on the value of δ . As δ decreases, the interfaces turn flat generally, and the whole process of phase transition approaches that of the diffuse interface described by the local case. On the contrary, the interfaces turn sharper and sharper as δ increases, but unlike the case of decreasing ε given above, the time needed for reaching the steady state turn a little shorter. Fig. 4 shows the results with fixed $\varepsilon = 0.05$ and $\delta^2 = 0.01$, 0.0075, 0.005, 0.0025, respectively, and the similar phenomena are observed.

According to the numerical results presented above, we find that, within the range of chosen parameters, the main influence of the horizon parameter δ concentrates only on the slope around the interface in the steady state, while the interfacial parameter ε , as its action in the local case, influences not only the slope of the interface, but also the height and shape of the “hill peak” away from the interface, and effectively the whole evolution of the phase transition.

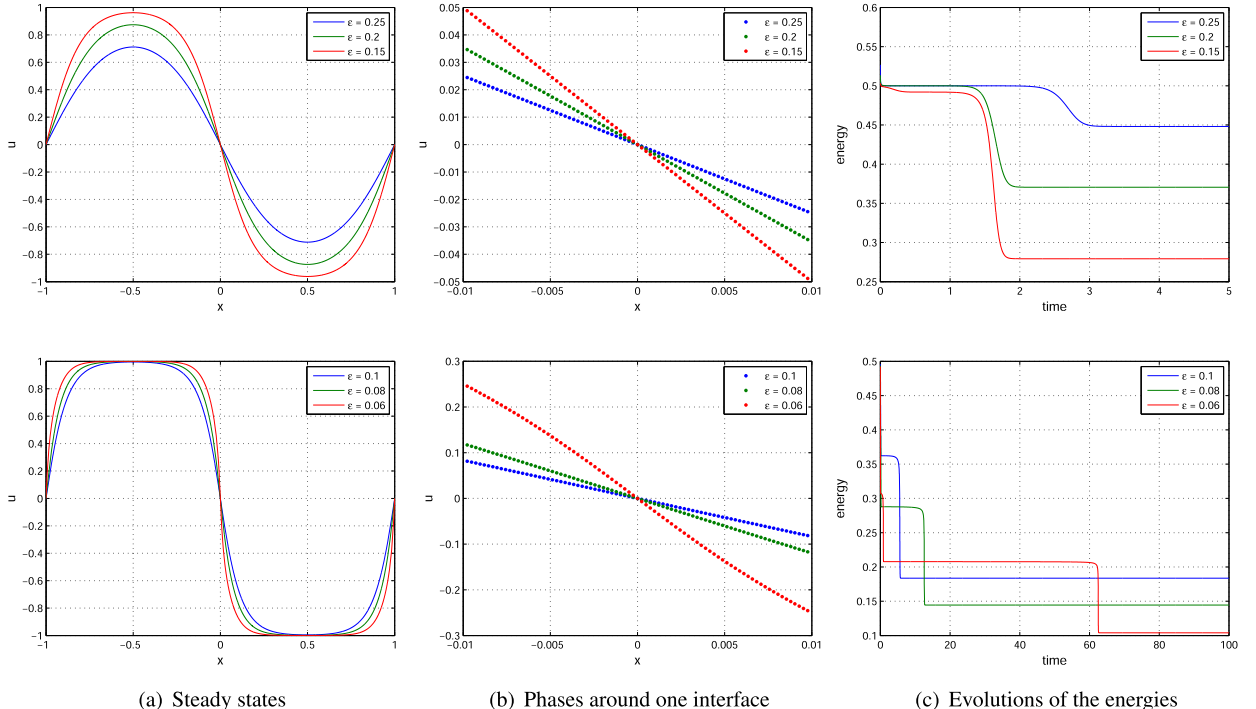


Fig. 2. Simulation results in Example 2 with $\delta^2 = 0.01$ and ϵ as 0.25, 0.2, 0.15 (top), 0.1, 0.08, 0.06 (bottom), respectively. (For interpretation of the colors in the figure, the reader is referred to the web version of this article.)

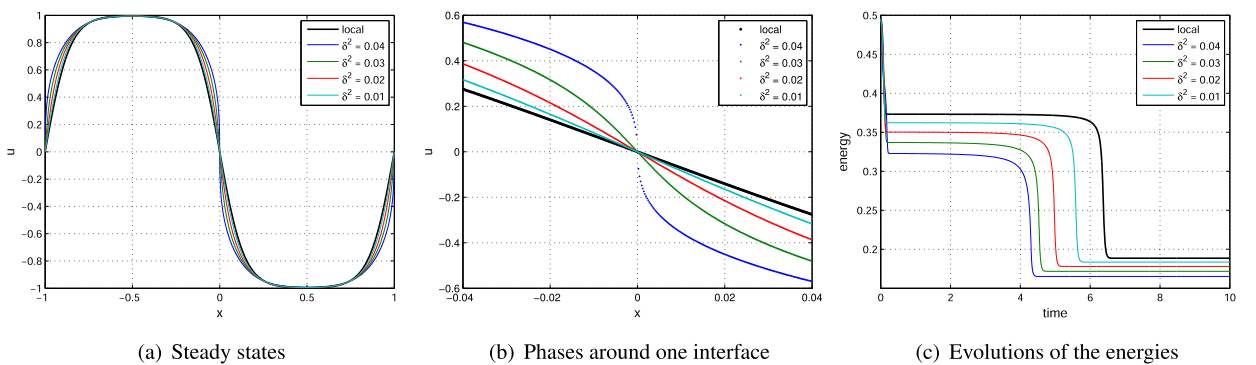


Fig. 3. Simulation results in Example 2 with $\epsilon = 0.1$ and $\delta^2 = 0.04, 0.03, 0.02$, and 0.01, respectively. (For interpretation of the colors in the figure, the reader is referred to the web version of this article.)

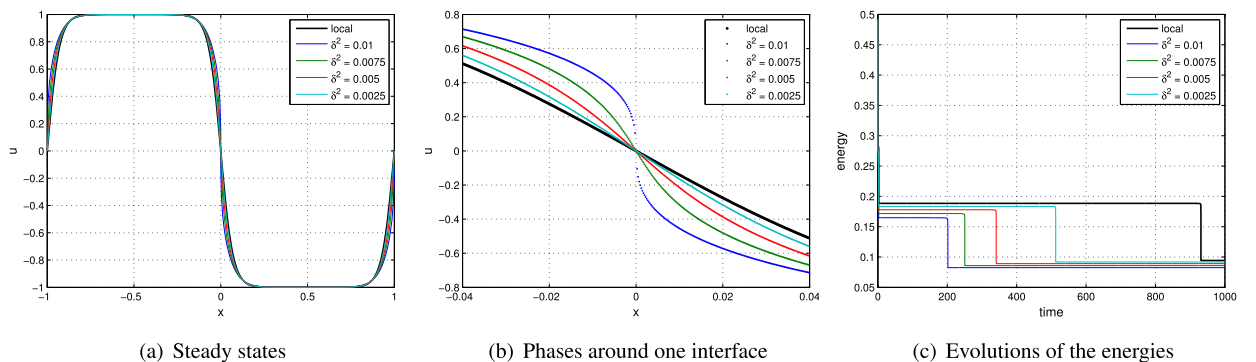


Fig. 4. Simulation results in Example 2 with $\epsilon = 0.05$ and $\delta^2 = 0.01, 0.0075, 0.005$, and 0.0025, respectively. (For interpretation of the colors in the figure, the reader is referred to the web version of this article.)

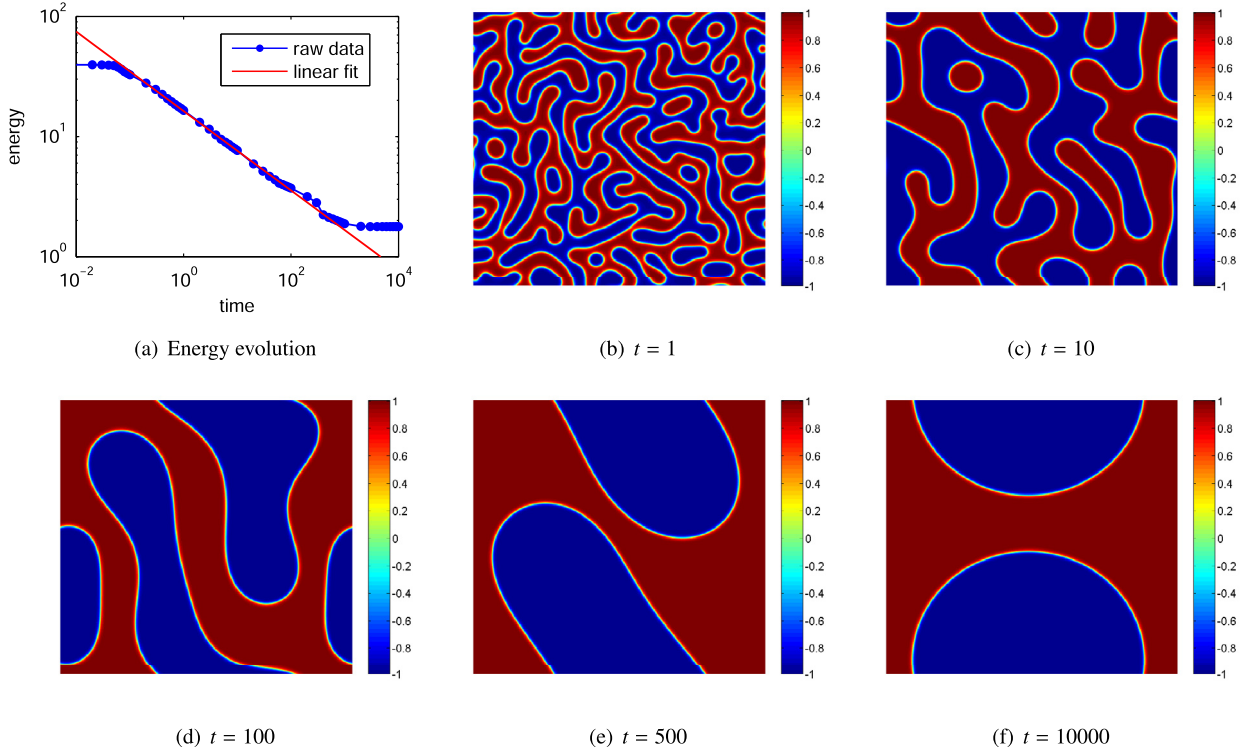


Fig. 5. Energy evolution with $\varepsilon = 0.09$ and the approximate solutions at different times in Example 3. (For interpretation of the colors in the figure, the reader is referred to the web version of this article.)

Table 1
Coefficients of the linear fitting for the case $\delta = \varepsilon$ with $N = 512$.

ε	0.09	0.08	0.07	0.06	0.05	0.04	0.03
m_e	-0.331	-0.333	-0.337	-0.340	-0.335	-0.336	-0.339
b_e	16.305	15.074	13.886	12.735	11.197	9.708	8.016

Table 2
Coefficients of the linear fitting for the case $\delta = 0.05$ with $N = 512$.

ε	0.1	0.09	0.08	0.07	0.06	0.05	0.04
m_e	-0.321	-0.320	-0.323	-0.336	-0.331	-0.340	-0.333
b_e	18.410	16.922	15.618	14.163	12.838	11.224	9.689

5.3. Coarsening dynamics

Example 3. We take $\Omega = (-2\pi, 2\pi) \times (-2\pi, 2\pi)$ and simulate the long time behavior of the phase transition using the SSI2 scheme. The initial configuration is a random state given by random numbers varying uniformly in $[-0.1, 0.1]$ on each point in the uniform mesh. We set the time step size $\tau = 0.001$ on the time interval $[0, 1000]$, $\tau = 0.01$ on $[1000, 10000]$, and $\tau = 0.1$ for $t \geq 10000$ if needed.

First, we consider the case of $\delta = \varepsilon$ and choose $N = 512$. Fig. 5 presents some numerical results for $\varepsilon = 0.09$. The first graph shows the linear fitting of the log-log energy data up to $t = 100$, where the fitting line is of the form $E(t) = b_e t^{m_e}$ with $m_e = -0.331$ and $b_e = 16.305$, which suggests the $t^{-\frac{1}{3}}$ power law for the energy decay rate. The rest five pictures give the configurations of the approximate solution at time 1, 10, 100, 500, and 10000. Table 1 presents the linear fitting coefficients m_e and b_e for the cases from $\varepsilon = 0.09$ to $\varepsilon = 0.03$. All the values of m_e are located around $-\frac{1}{3}$.

Next, we fix $\delta = 0.05$ with $N = 512$ and decrease ε from 0.1 to 0.04. The linear fitting coefficients are listed in Table 2 and the energies are partially plotted in Fig. 6(a). It can be found that the energy decay rates comply with the $-1/3$ power law quite well for all cases. This is consistent to the local Cahn–Hilliard dynamics, see [13,28] for further discussions and

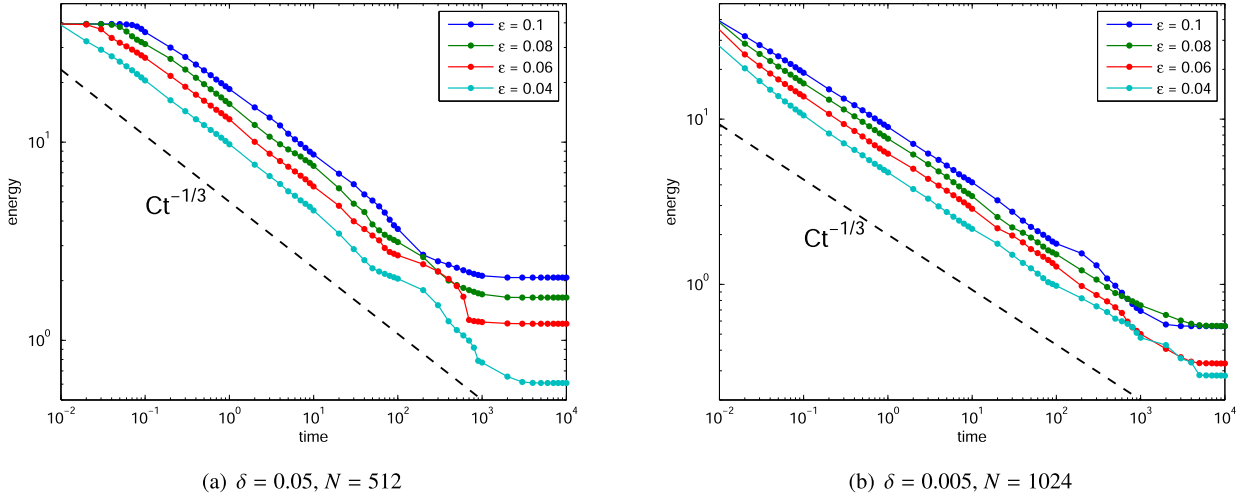


Fig. 6. Evolutions of the energies in Example 3.

Table 3
Coefficients of the linear fitting for the case $\delta = 0.005$ with $N = 1024$.

ε	0.1	0.09	0.08	0.07	0.06	0.05	0.04
m_e	−0.333	−0.346	−0.340	−0.344	−0.339	−0.344	−0.342
b_e	8.932	8.231	7.611	6.960	6.245	5.473	4.756

additional references. The results for the case $\delta = 0.005$ with $N = 1024$ are presented in Table 3 and Fig. 6(b) and the similar behavior is again observed.

6. Concluding remarks

In this paper, we investigate both first and second order stabilized linear semi-implicit schemes for the NCH equation. Under the assumption on the positivity of the kernel, we treat the nonlocal diffusion term implicitly while the nonlinear term explicitly, and add a stabilizing term to obtain the stabilized schemes. For each scheme, we prove the energy stability when the stabilizer A is sufficiently large, depending on the discrete L^∞ bound of the numerical solutions. Numerical experiments are conducted with the Gaussian kernels parameterized by δ to demonstrate the optimal convergence rates in time, to investigate the phase transition interfaces of steady states with different choices of ε and δ , and to predict the $-\frac{1}{3}$ power law for the energy decay in the long time evolutions. The numerical results show that the interfaces become sharper when ε decreases or δ increases, and it takes longer time for the evolution to reach the steady state for smaller ε .

The problem we consider in this work is obtained by replacing the Laplacian in the local energy (9) by the nonlocal diffusion operator \mathcal{L}_h defined as (2). In order to ensure the diffusivity of the problem, we assume that the kernel is integrable and its integral value is greater than $1/\varepsilon^2$, though such assumptions are unnecessary to prove the energy stability, which implies that the same results for the cases with more general kernels are still held. Here we consider the integrable kernel just to make the computations simpler. Indeed, the case with non-integrable kernels will be distinct and worthy further investigation, and the eigenvalues of more general nonlocal operators could be computed by a hybrid algorithm proposed in [17]. In addition, we also could replace the Laplacian in (5) by another nonlocal operator to obtain the NCH equation in a more general form, and consider their numerical analysis as one of our future works. Further extensions can also be made to include variable (and concentration dependent) mobilities as in the local case [28].

It is worth noting that we make an assumption on the uniform boundness of the numerical solutions so that we can develop the energy stabilities for the proposed stabilized schemes. As mentioned in the remark following Theorem 1, such a condition is equivalent to the Lipschitz continuity of the derivative of the potential. In recent works [29,30], a new condition on the stabilizer A is provided, where neither the uniform boundness nor the Lipschitz continuity is needed. It remains to be further studied if the similar approach can be utilized for the NCH equation with suitable kernels. Moreover, error estimates for these fully discrete schemes also remain to be investigated in the future work.

Acknowledgements

Q. Du's work is partially supported by US National Science Foundation grant DMS-1719699, US AFOSR MURI Center for Material Failure Prediction Through Peridynamics grant FA9550-14-1-0073, and US Army Research Office MURI grant W911NF-15-1-0562. L. Ju's work is partially supported by US National Science Foundation grant DMS-1521965 and U.S.

Department of Energy grant DE-SC0016540. X. Li's work is partially supported by China Postdoctoral Science Foundation grant 2017M610748. Z. Qiao's work is partially supported by the Hong Kong Research Council GRF grants 15325816 and 15300417 and the Hong Kong Polytechnic University fund 1-ZE33.

References

- [1] A. Archer, R. Evans, Dynamical density functional theory and its application to spinodal decomposition, *J. Chem. Phys.* 121 (2004) 4246–4254.
- [2] A. Archer, M. Rauscher, Dynamical density functional theory for interacting Brownian particles: stochastic or deterministic?, *J. Phys. A: Math. Gen.* 37 (2004) 9325.
- [3] S. Armstrong, S. Brown, J.L. Han, Numerical analysis for a nonlocal phase field system, *Int. J. Numer. Anal. Model. Ser. B* 1 (2010) 1–9.
- [4] P.W. Bates, On some nonlocal evolution equations arising in materials science, *Fields Inst. Commun.* 48 (2006) 13–52.
- [5] P.W. Bates, S. Brown, J.L. Han, Numerical analysis for a nonlocal Allen–Cahn equation, *Int. J. Numer. Anal. Model.* 6 (2009) 33–49.
- [6] P.W. Bates, A.J. Chmaj, An integrodifferential model for phase transitions: stationary solutions in higher space dimensions, *J. Stat. Phys.* 95 (1999) 1119–1139.
- [7] P.W. Bates, J.-L. Han, The Neumann boundary problem for a nonlocal Cahn–Hilliard equation, *J. Differ. Equ.* 212 (2005) 235–277.
- [8] P.W. Bates, J.-L. Han, The Dirichlet boundary problem for a nonlocal Cahn–Hilliard equation, *J. Math. Anal. Appl.* 311 (2005) 289–312.
- [9] J. Bourgain, H. Brezis, P. Mironescu, Another look at Sobolev spaces, in: *Optimal Control and Partial Differential Equations*, IOS Press, Amsterdam, 2001, pp. 439–455.
- [10] J.W. Cahn, J.E. Hilliard, Free energy of a nonuniform system I. Interfacial free energy, *J. Chem. Phys.* 28 (1958) 258–267.
- [11] L.-Q. Chen, J. Shen, Applications of semi-implicit Fourier-spectral method to phase field equations, *Comput. Phys. Commun.* 108 (1998) 147–158.
- [12] W.-B. Chen, S. Conde, C. Wang, X.-M. Wang, S.M. Wise, A linear energy stable scheme for a thin film model without slope selection, *J. Sci. Comput.* 52 (2012) 546–562.
- [13] S.-B. Dai, Q. Du, Computational studies of coarsening rates of the Cahn–Hilliard equation with phase-dependent diffusion mobility, *J. Comput. Phys.* 310 (2016) 85–108.
- [14] Q. Du, M. Gunzburger, R. Lehoucq, K. Zhou, Analysis and approximation of nonlocal diffusion problems with volume constraints, *SIAM Rev.* 54 (2012) 667–696.
- [15] Q. Du, M. Gunzburger, R. Lehoucq, K. Zhou, A nonlocal vector calculus, nonlocal volume-constrained problems, and nonlocal balance laws, *Math. Models Methods Appl. Sci.* 23 (2013) 493–540.
- [16] Q. Du, J. Yang, Asymptotically compatible Fourier spectral approximations of nonlocal Allen–Cahn equations, *SIAM J. Numer. Anal.* 54 (2016) 1899–1919.
- [17] Q. Du, J. Yang, Fast and accurate implementation of Fourier spectral approximations of nonlocal diffusion operators and its applications, *J. Comput. Phys.* 332 (2017) 118–134.
- [18] C.M. Elliott, S.-M. Zheng, On the Cahn–Hilliard equation, *Arch. Ration. Mech. Anal.* 96 (1986) 339–357.
- [19] D.J. Eyre, Unconditionally gradient stable time marching the Cahn–Hilliard equation, in: J.W. Bullard, R. Kalia, M. Stoneham, L.Q. Chen (Eds.), *Computational and Mathematical Models of Microstructural Evolution*, in: Mater. Res. Soc. Symp. Proc., vol. 529, Materials Research Society, Warrendale, PA, 1998, pp. 39–46.
- [20] P.C. Fife, Some nonclassical trends in parabolic and parabolic-like evolutions, in: *Trends in Nonlinear Analysis*, Springer, Berlin, 2003, pp. 153–191.
- [21] H. Gajewski, K. Gärtner, On a nonlocal model of image segmentation, *Z. Angew. Math. Phys.* 56 (2005) 572–591.
- [22] Z. Guan, J.S. Lowengrub, C. Wang, Convergence analysis for second order accurate schemes for the periodic nonlocal Allen–Cahn and Cahn–Hilliard equations, *Math. Methods Appl. Sci.* 40 (2017) 6836–6863.
- [23] Z. Guan, J.S. Lowengrub, C. Wang, S.M. Wise, Second order convex splitting schemes for periodic nonlocal Cahn–Hilliard and Allen–Cahn equations, *J. Comput. Phys.* 277 (2014) 48–71.
- [24] Z. Guan, C. Wang, S.M. Wise, A convergent convex splitting scheme for the periodic nonlocal Cahn–Hilliard equation, *Numer. Math.* 128 (2014) 377–406.
- [25] Y.-N. He, Y.-X. Liu, T. Tang, On large time-stepping methods for the Cahn–Hilliard equation, *Appl. Numer. Math.* 57 (2007) 616–628.
- [26] D. Horntrop, M. Katsoulakis, D. Vlachos, Spectral methods for mesoscopic models of pattern formation, *J. Comput. Phys.* 173 (2001) 364–390.
- [27] L. Ju, X. Li, Z.-H. Qiao, H. Zhang, Energy stability and error estimates of exponential time differencing schemes for the epitaxial growth model without slope selection, *Math. Comput.* (2018), <https://doi.org/10.1090/mcom/3262>, in press.
- [28] L. Ju, J. Zhang, Q. Du, Fast and accurate algorithms for simulating coarsening dynamics of Cahn–Hilliard equations, *Comput. Mater. Sci.* 108 (2015) 272–282.
- [29] D. Li, Z.-H. Qiao, On second order semi-implicit Fourier spectral methods for 2D Cahn–Hilliard equations, *J. Sci. Comput.* 70 (2017) 301–341.
- [30] D. Li, Z.-H. Qiao, T. Tang, Characterizing the stabilization size for semi-implicit Fourier-spectral method to phase field equations, *SIAM J. Numer. Anal.* 54 (2016) 1653–1681.
- [31] T. Mengesha, Q. Du, On the variational limit of a class of nonlocal functionals related to peridynamics, *Nonlinearity* 28 (2015) 3999–4035.
- [32] R.C. Merton, Option pricing when underlying stock returns are discontinuous, *J. Financ. Econ.* 3 (1976) 125–144.
- [33] L.M. Pismen, Nonlocal diffuse interface theory of thin films and the moving contact line, *Phys. Rev. E* 64 (2001) 021603.
- [34] Z.-H. Qiao, S.-Y. Sun, Two-phase fluid simulation using a diffuse interface model with Peng–Robinson equation of state, *SIAM J. Sci. Comput.* 36 (2014) B708–B728.
- [35] Z.-H. Qiao, Z.-Z. Sun, Z.-R. Zhang, Stability and convergence of second-order schemes for the nonlinear epitaxial growth model without slope selection, *Math. Comput.* 84 (2015) 653–674.
- [36] Z.-H. Qiao, Z.-R. Zhang, T. Tang, An adaptive time-stepping strategy for the molecular beam epitaxy models, *SIAM J. Sci. Comput.* 33 (2011) 1395–1414.
- [37] J. Shen, T. Tang, L.-L. Wang, *Spectral Methods: Algorithms, Analysis and Applications*, Springer, Berlin, 2011.
- [38] J. Shen, X.-F. Yang, Numerical approximations of Allen–Cahn and Cahn–Hilliard equations, *Discrete Contin. Dyn. Syst.* 28 (2010) 1669–1691.
- [39] X.-C. Tian, Q. Du, Analysis and comparison of different approximations to nonlocal diffusion and linear peridynamic equations, *SIAM J. Numer. Anal.* 51 (2013) 3458–3482.
- [40] X.-C. Tian, Q. Du, Asymptotically compatible schemes for robust discretization of nonlocal models and their local limits, *SIAM J. Numer. Anal.* 52 (2014) 1641–1665.
- [41] L.N. Trefethen, *Spectral Methods in MATLAB*, SIAM, Philadelphia, 2000.
- [42] J.D. van der Waals, The thermodynamic theory of capillarity under the hypothesis of a continuous variation of density, *J. Stat. Phys.* 20 (1979) 200–244.
- [43] C. Wang, S.M. Wise, J.S. Lowengrub, An energy-stable and convergent finite-difference scheme for the phase field crystal equation, *SIAM J. Numer. Anal.* 47 (2009) 2269–2288.
- [44] C.-J. Xu, T. Tang, Stability analysis of large time-stepping methods for epitaxial growth models, *SIAM J. Numer. Anal.* 44 (2006) 1759–1779.
- [45] K. Zhou, Q. Du, Mathematical and numerical analysis of linear peridynamic models with nonlocal boundary conditions, *SIAM J. Numer. Anal.* 48 (2010) 1759–1780.